A&A 533, A113 (2011)
DOI: 10.1051/0004-6361/201116760

Astronomy & Astrophysics

Spin-orbit inclinations of the exoplanetary systems HAT-P-8b, HAT-P-9b, HAT-P-16b, and HAT-P-23b ⋆

C. Moutou[1], R. F. Díaz[2,3], S. Udry[4], G. Hébrard[2,3], F. Bouchy[2,3], A. Santerne[1,3], D. Ehrenreich[5], L. Arnold[3], I. Boisse[2,6], X. Bonfils[5], X. Delfosse[5], A. Eggenberger[5], T. Forveille[5], A.-M. Lagrange[5], C. Lovis[4], P. Martinez[7], F. Pepe[4], C. Perrier[5], D. Queloz[4], N. C. Santos[6,10], D. Ségransan[4], D. Toublanc[7,8], J. P. Troncin[3], M. Vanhuysse[9], and A. Vidal-Madjar[2]

[1] Laboratoire d'Astrophysique de Marseille, UMR 6110, OAMP, CNRS and Univ. de Provence, 38 rue Frédéric Joliot-Curie, 13388 Marseille Cedex 13, France
e-mail: Claire.Moutou@oamp.fr
[2] Institut d'Astrophysique de Paris, UMR 7095 CNRS, Université Pierre and Marie Curie, 98bis boulevard Arago, 75014 Paris, France
[3] Observatoire de Haute-Provence, CNRS and OAMP, 04870 Saint-Michel l'Observatoire, France
[4] Observatoire de Genève, Université de Genève, 51 Chemin des Maillettes, 1290 Sauverny, Switzerland
[5] UJF-Grenoble 1 / CNRS-INSU, Institut de Planétologie et d'Astrophysique de Grenoble (IPAG) UMR 5274, Grenoble 38041, France
[6] Centro de Astrofísica, Universidade do Porto, Rua das Estrelas, 4150-762 Porto, Portugal
[7] Association Adagio, L'Observatoire, 31540 Belesta Lauragais, France
[8] Université Toulouse III, UMR5187, 118 route de Narbonne 31062 Toulouse, France
[9] Oversky, 47 Allée des Palanques, 33127 Saint Jean d'Illac, France
[10] Departamento de Física e Astronomia, Faculdade de Ciências, Universidade do Porto, Portugal

Received 21 February 2011 / Accepted 18 May 2011

ABSTRACT

We report the measurement of the spin-orbit angle of the extra-solar planets HAT-P-8 b, HAT-P-9 b, HAT-P-16 b, and HAT-P-23 b, based on spectroscopic observations performed at the Observatoire de Haute-Provence with the SOPHIE spectrograph on the 1.93-m telescope. Radial velocity measurements of the Rossiter-McLaughlin effect show the detection of an apparent prograde, aligned orbit for all systems. The projected spin-orbit angles are found to be $\lambda = -17^{\circ}{}^{+9.2}_{-11.5}$, $-16^{\circ} \pm 8^{\circ}$, $-10^{\circ} \pm 16^{\circ}$, and $+15^{\circ} \pm 22^{\circ}$ for HAT-P-8, HAT-P-9, HAT-P-16, and HAT-P-23, respectively, with corresponding projected rotational velocities of 14.5 ± 0.8, 12.5 ± 1.8, 3.9 ± 0.8, and 7.8 ± 1.6 km s^{-1}. These new results increase to 37 the number of accurately measured spin-orbit angles in transiting extrasolar systems. We conclude by drawing a tentative picture of the global behaviour of orbital alignement, involving the complexity and diversity of possible mechanisms.

Key words. techniques: radial velocities – planet-star interactions – planetary systems

1. Introduction

The number of extrasolar planetary systems that have been discovered is ever increasing, at a rate of higher than 50 per year since 2007[1]. The sub-sample of confirmed transiting systems (∼100) is then subsequently explored with greater care, since the measurement of their real mass and radius allows us to study their internal structure. For a sub-group of transiting systems, several teams have now collected the observation of spectroscopic transits with high-precision radial-velocity instruments, giving us access to the relative angle between the stellar spin plane and the planetary orbital plane through the modelling of the Rossiter-McLaughlin effect (Rossiter 1924). Unexpectedly, one third of the short-period planets for which those measurements are available have significantly misaligned orbits with respect to their star's rotational axis, even polar or retrograde (e.g., Triaud et al. 2010; Hébrard et al. 2010; Winn et al. 2010a). This distribution of stellar obliquities is consistent with a scenario of formation and orbital evolution of extrasolar giant planets that is more diverse than pure one-planet migration inside a proto-planetary disk.

In this paper, we report the Rossiter-McLaughlin measurement of four additional transiting planets, HAT-P-8 b, HAT-P-9 b, HAT-P-16 b, and HAT-P-23 b, performed using data obtained at Observatoire de Haute Provence with the SOPHIE high-precision radial-velocity (RV) spectrograph. The four systems discussed here are transiting extrasolar planets found by the HATNet photometric survey (Bakos et al. 2002, 2004).

HAT-P-8 b is an inflated hot Jupiter, with a mass $M_{\rm p}$= 1.52 $M_{\rm Jup}$, a radius $R_{\rm p}$= 1.50 $R_{\rm Jup}$ and a circular orbit of period 3.076 days (Latham et al. 2009). The host star HAT-P-8 is a solar-metallicity F main-sequence star with a significant projected velocity of about 12 km s^{-1}, and magnitude V = 10.17.

HAT-P-9 is an inflated, moderate-mass Jupiter-like planet, with $M_{\rm p}$ = 0.78 $M_{\rm Jup}$ and $R_{\rm p}$ = 1.4 $R_{\rm Jup}$. It orbits a late F star in a 3.92289-day circular orbit (Shporer et al. 2009). The star

⋆ Based on observations collected with the SOPHIE spectrograph on the 1.93-m telescope at Observatoire de Haute-Provence (CNRS), France, by the SOPHIE Consortium (program 10A.PNP.CONS).
[1] http://www.encyclopedia.edu

is relatively faint, with $V = 12.3$. The determination of its ephemeris has been revisited (Dittmann et al. 2010) and we used the updated value for the observation scheduling and transit modeling.

HAT-P-16 b is a 4 $M_{\rm Jup}$ planet transiting a $V = 10.8$ mag star; its orbital period is 2.77596 days, its radius is 1.29 $R_{\rm Jup}$, and it has a slightly eccentric orbit despite its short period ($e = 0.036$ with a 10σ significance). The parent star has a mass of 1.2 $M_{\odot}$ and an effective temperature of 6158 K (Buchhave et al. 2010).

HAT-P-23 b is an inflated and massive giant planet orbiting a G0 dwarf star with $V = 11.94$, in 1.212884d. Its mass and radius are 2.09 $M_{\rm Jup}$ and 1.37 $R_{\rm Jup}$; although the orbital period is extremely short, the orbit of HAT-P-23 b is slightly but significantly eccentric, with $e = 0.106$. Its detection and analysis were reported by Bakos et al. (2010).

Section 2 describes the spectroscopic observations, Sect. 3 presents additional photometry that was performed and analysed to refine the ephemeris of HAT-P-8 b, Sect. 4 discusses the modeling of the Rossiter-McLaughlin effect. In Sect. 5, we put these discoveries into context and discuss the global picture of orbital alignment.

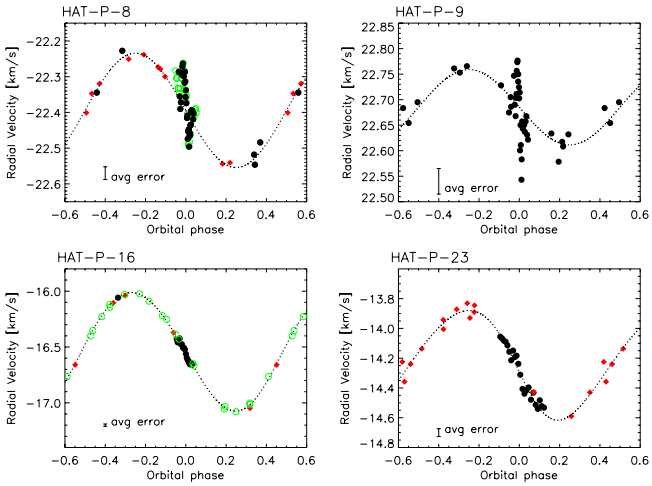

Fig. 1. SOPHIE (black plain circles), Keck/HIRES (red diamonds), FIES (open green circles) radial-velocity data of HAT-P-8, HAT-P-9, HAT-P-16, and HAT-P-23. The superimposed orbital solution is our best-fit to the data (not including the spectroscopic transits in this plot).

Table 1. Updated orbit and planetary parameters for HAT-P-8 b.

Parameters	Values and 1-σ error bars	Unit
$V_{\rm r}$ (SOPHIE)	–22.383 ± 0.01	km s^{-1}
P	3.0763373 ± 0.0000031	days
K	158.2 ± 3.2	m s^{-1}
$M_{\rm p}$	1.34 ± 0.05	$M_{\rm Jup}$
a	0.0449 ± 0.0007	AU
$T_{\rm t}$ (primary transit)	2454437.67505 ± 0.00042	BJD

Notes. A circular orbit is assumed.

2. Spectroscopic observations

The spectroscopic observations were obtained at Observatoire de Haute Provence with the 1.93 m telescope, in the framework of the large program (reference 10A.PNP.CONS) led by the SOPHIE Consortium, presented in detail by Bouchy et al. (2009a). The SOPHIE instrument (Perruchot et al. 2008) is a fiber-fed environmentally stabilized echelle spectrograph covering the visible range from 387 to 694 nm. The spectral resolving power is 70 000 in the high resolution mode, and 40 000 in the high efficiency mode. For high-cadence observations required in a Rossiter sequence, the limit between both modes is around $V = 9.5-10$: the gain in resolution does not compensate for the increase in the readout noise for fainter stars.

The observing template "objAB" is used, in order to simultaneously monitor the sky background contamination. A correction for this background is required when the sky brightness is high and the Earth velocity does not differ sufficiently from the stellar velocity.

The radial velocities are obtained by cross-correlating the 2D extracted spectra with a stellar numerical mask, following the method developed by Baranne et al. (1996).

2.1. HAT-P-8

The transit of HAT-P-8 b was observed during the night of 19 July 2010. We observed the $V = 10.17$ mag HAT-P-8 star in the high efficiency mode, and slow readout mode to reduce the detector noise. Three measurements of this target were collected in 2009, and three in 2010 outside the transit night. These few measurements permitted us to combine with a properly defined offset the orbital radial-velocity variations to the set of higher-accuracy Keck/HIRES data described in Latham et al. (2009). During the transit night (around JD = 55 397.5), we secured 35 measurements, between 21:40 to 02:40 UT. Their signal-to-noise ratios range from 37 to 42, with exposure times from 220 to 640 s. Observing to ensure a constant signal-to-noise ratio (hereafter S/N) with SOPHIE allows us to reduce the radial-velocity systematics, which are caused by the illumination-sensitive charge transmission efficiency (Bouchy et al. 2009b). Although this systematic effect can be efficiently corrected after the proper calibration effect has been quantified, by observing at constant S/N we reduce this effect. The individual error bars range from 16 m/s to 21 m/s. The six bluest orders were removed from the velocity calculation, since they add only noise, and the G2 mask was used for the cross-correlation. The 1-σ error bar of our measurements collected within transit is 18 m/s, which is similar to the error in the measurements collected outside transit.

The RV data of HAT-P-8 presented in this paper are given in Table 2 and shown in Fig. 1, together with the previous Keck/HIRES data of Latham et al. (2009). They are phased to the ephemeris refined by our photometric observations (see Sect. 3). Modelling the full out-of-transit radial-velocity sequence using both Keck and SOPHIE data with a Keplerian solution, we find a semi-amplitude of the variation that is 1.5-σ larger than in Latham et al. (2009), and values for the planetary mass and the semi-major axis that vary accordingly. We update the orbital parameters and planetary mass in Table 1. The eccentricity being compatible with zero at less than the 2-σ level, we assume here a circular orbit, as in Latham et al. (2009). The bisector span is constant to the 2-σ level during the sequence.

The velocity anomaly during the transit has an amplitude that is only 30% smaller than the orbital amplitude; this was expected on the basis of the significant projected velocity of the star and the large planetary radius (11.5 km s^{-1} and 1.5 $R_{\rm Jup}$, respectively, in Latham et al. 2009). This $v \sin i_{\rm s}$ can also be estimated from the cross-correlation function, as described in Boisse et al. (2010). We find that $v \sin i_{\rm s} = 12.9 \pm 1$ km s^{-1}, which is larger but in agreement with the value reported in Latham et al. (2009).

Table 2. Radial velocity measurements obtained with SOPHIE of HAT-P-8.

JD-2 400 000	Radial vel. [km s^{-1}]	Uncertainty [m s^{-1}]
55 072.45560	–22.5463	18.4
55 080.52188	–22.2864	18.5
55 088.49962	–22.3445	18.9
55 395.55227	–22.4840	20.8
55 396.52298	–22.2275	17.8
55 397.39997	–22.3553	18.5
55 397.40930	–22.3904	18.0
55 397.41822	–22.3718	18.6
55 397.43378	–22.2944	17.6
55 397.44022	–22.2714	17.5
55 397.44685	–22.2634	17.5
55 397.45327	–22.2887	18.3
55 397.46034	–22.2989	17.8
55 397.46719	–22.2869	17.2
55 397.47357	–22.3169	17.3
55 397.47896	–22.2864	17.1
55 397.48420	–22.3135	17.1
55 397.48938	–22.3570	17.5
55 397.49458	–22.3382	17.4
55 397.50028	–22.3741	17.3
55 397.51130	–22.4156	17.5
55 397.51675	–22.4090	17.5
55 397.52222	–22.4740	17.7
55 397.52780	–22.4527	17.8
55 397.53327	–22.4539	17.6
55 397.53856	–22.4475	17.8
55 397.54369	–22.4959	17.6
55 397.54868	–22.4662	17.7
55 397.55407	–22.4575	17.5
55 397.55914	–22.4639	17.6
55 397.56427	–22.4359	18.0
55 397.56930	–22.4345	18.1
55 397.57425	–22.3988	18.1
55 397.57918	–22.3946	18.4
55 397.58403	–22.3932	18.5
55 397.58884	–22.3961	18.3
55 397.59440	–22.3973	18.6
55 397.59935	–22.3989	18.5
55 397.60439	–22.4194	18.4
55 397.60947	–22.4037	18.4
55 398.53561	–22.5182	15.5

2.2. HAT-P-9

Two partial transits of HAT-P-9 were recorded, on 28 December 2010 and 1 January 2011 in the high efficiency mode and slow readout. Ten (seventeen) measurements were secured during the first (respectively second) night. Exposure times ranging from 830 to 1200 s resulted in spectra with S/N ranging from 14 to 31. An error of 12 m/s was quadratically added to the photon noise uncertainty, to account for instrumental systematics at low S/N and to obtain a final χ^2 value of close to 1 for the orbital fitting. We added the fifteen measurements obtained with SOPHIE in 2007–2008, at the planet's discovery by Shporer et al. (2009). All spectra were reduced in the same way, using the F0 correlation mask and spectrograph orders from 3 to 34. The values are reported in Table 3. We finally adjusted the planetary orbit using the last ephemeris derived by additional photometry by Dittmann et al. (2010). All RV data are shown in Fig. 1.

The transit-center epochs, using this ephemeris, are expected at Julian dates 5559.44531 and 245 563.37109. Owing to variations in the weather conditions, we had to interrupt the first sequence 30 min before the end of the transit, and we did not get data after the transit on the 28 December 2010 (observations lasted from 20:17 to 23:54 UT). The second sequence nicely completes the first one, with a full transit being observed and seven measurements being possible after transit (from 19:20 to 00:59 UT). No data were obtained however before transit, because of the twilight. The radial-velocity time series of both transits were assembled by allowing for a free offset between both sequences, to accomodate an observed shift of 37 m/s. The reason for this may be related to the atmospheric chromatic disperser setup. This does not, however, cause additional jitter during the short timescale of the transit itself, thus all data are kept in the fit. The bisector span is constant at the 1.6-σ level during the sequence. The average width of the cross-correlation function is 16.6 km s^{-1}, which corresponds to a projected rotational velocity of 12.2 km s^{-1}, with a precision of about 1 km s^{-1}. This value is compatible with the one found by Shporer et al. (2009) from the analysis of stellar parameters (11.9 ± 1 km s^{-1}).

Table 3. Radial velocity measurements obtained with SOPHIE of HAT-P-9.

JD-2 400 000	Radial vel. [km s^{-1}]	Uncertainty [m s^{-1}]
55 559.34192	22.6812	36.9
55 559.35866	22.5790	43.2
55 559.37506	22.5852	33.5
55 559.39135	22.6719	35.1
55 559.40763	22.6588	34.0
55 559.42391	22.6997	28.8
55 559.44366	22.6173	34.0
55 559.46000	22.5507	37.2
55 559.47627	22.5503	35.2
55 559.49255	22.5119	56.9
55 563.30211	22.6347	32.3
55 563.31818	22.6929	33.5
55 563.33464	22.7358	27.9
55 563.34868	22.7057	27.4
55 563.36333	22.6758	28.9
55 563.37770	22.6792	28.5
55 563.39233	22.6012	29.1
55 563.41194	22.5295	28.1
55 563.42434	22.5684	28.4
55 563.43747	22.6301	31.1
55 563.45125	22.6167	26.0
55 563.46384	22.5940	26.2
55 563.47781	22.6040	25.1
55 563.49242	22.6422	24.5
55 563.50598	22.6353	24.3
55 563.52041	22.5892	23.8
55 563.53780	22.5987	23.7

2.3. HAT-P-16

The transit of HAT-P-16 b was observed during the night of 15 August 2010 with SOPHIE in the high resolution mode and fast readout mode (Table 4). To ensure that the S/N remained constant (~27 ± 1) over the five-hour sequence, an exposure time of 848 to 1400 s was used. The cross-correlation is calculated with a G2 mask, which reduces the size of the individual error bars, excluding the 14 bluest orders to diminish the systematic effects due to an incorrect positioning of the atmospheric chromatic disperser during this observation. A RV precision of 10 to 15 m/s was achieved. The stellar spectrum was unaffected by any significant background light. One additional

Table 4. Radial velocity measurements obtained with SOPHIE of HAT-P-16.

JD-2 400 000	Radial vel. [km s^{-1}]	Uncertainty [m s^{-1}]
55 424.43002	–16.4335	10.7
55 424.44167	–16.4491	10.4
55 424.45587	–16.4358	12.5
55 424.47137	–16.4391	15.4
55 424.48567	–16.5030	15.4
55 424.50068	–16.4913	14.5
55 424.51498	–16.5081	11.6
55 424.52851	–16.5096	10.8
55 424.54198	–16.5225	11.2
55 424.55597	–16.5680	11.3
55 424.56858	–16.5967	11.0
55 424.57975	–16.6180	10.9
55 424.59027	–16.6271	10.9
55 424.60097	–16.6502	10.9
55 424.61203	–16.6542	11.1
55 424.62317	–16.6594	10.8
55 424.63377	–16.6644	10.9
55 424.64422	–16.6681	10.8

measurement for data obtained during the night before the transit in order to assess the RV uncertainty. Eighteen measurements were secured during the transit night. The sequence lasted from 22:19 to 03:27 UT. The transit was expected to occur between 23:47 and 02:51 UT, according to the ephemeris in Buchhave et al. (2010). The amplitude of the RV anomaly is extremely small, and the pattern appears regular as for a prograde aligned orbit, with a redshift followed by a blueshift. Figure 1 shows the SOPHIE data overplotted with literature data obtained with FIES and HIRES (Buchhave et al. 2010). The bisector span is constant to within 1.4-σ during the sequence.

A projected stellar rotational velocity of 3.0 ± 1 km s^{-1} is found by fitting the cross-correlation function, in agreement with the value reported in Buchhave et al. (2010) (3.5 ± 0.5 km s^{-1}).

2.4. HAT-P-23

The transit of HAT-P-23 b was observed during the night of 25 August 2010, a few days after its announcement by Bakos et al. (2011). In this sequence, SOPHIE was used in the high efficiency mode and fast readout mode. To ensure that the S/N remained constant (~24±1) over the 6.3-h sequence, an exposure time of 787 to 1200 s was used. A RV precision of from 24 m/s to 36 m/s has been obtained, after cross-correlating with the G2 mask, including all orders. Owing to the full Moon, a significant background contamination entered the spectrograph fibers. The stellar spectrum is a posteriori corrected for this effect, using the neighbouring fiber to monitor the sky flux simultaneously to each exposure. The value of the correction varies from 100 m/s to 500 m/s during the sequence, increasing towards the end of the sequence when the moon light became more prominent. The velocity difference between the barycentric Earth RV and the target's RV is about 5 km s^{-1} during the transit night. This contamination by background light induces a residual jitter in the last data points of the series, but does not prevent the detection of the RM anomaly, as seen in Fig. 1. The sequence on 25 August lasted from 20:01 to 02:20 UT, with a transit being expected from 21:41 to 23:51 UT following the ephemeris of Bakos et al. (2010). Twenty-three measurements were obtained during the transit night, plus one additional measurement two nights before

Table 5. Radial velocity measurements obtained with SOPHIE of HAT-P-23.

JD-2 400 000	Radial vel. [km s^{-1}]	Uncertainty [m s^{-1}]
55 434.33411	–14.0555	24.5
55 434.34457	–14.0666	25.6
55 434.35558	–14.0820	24.5
55 434.36645	–14.0898	24.9
55 434.37731	–14.1137	25.2
55 434.38856	–14.1572	26.2
55 434.40002	–14.2141	26.1
55 434.41127	–14.1490	25.6
55 434.42196	–14.1922	25.3
55 434.43227	–14.1831	25.4
55 434.44326	–14.2378	25.8
55 434.45460	–14.3113	26.1
55 434.46798	–14.4068	27.1
55 434.47968	–14.4386	25.5
55 434.49150	–14.4160	25.5
55 434.50469	–14.3966	26.2
55 434.51904	–14.4791	27.4
55 434.53355	–14.4316	26.9
55 434.54732	–14.5136	25.9
55 434.55997	–14.5404	27.2
55 434.57210	–14.4825	24.5
55 434.58393	–14.5221	29.0
55 434.59768	–14.5325	35.7

the transit (Table 5). The amplitude of the RM anomaly is of the order of 100 m/s and the orbit is prograde. Keck/HIRES radial velocities were added to our data set in order to simultaneously fit the orbit and the transit (Fig. 1 and Sect. 4). The bisector span is constant to within 1σ during the sequence.

We measure a projected stellar rotational velocity of 10 ± 1 km s^{-1}, which is larger by 2-σ than the value of 8.1 ± 0.5 km s^{-1} reported in Bakos et al. (2010).

3. Additional photometry

The observation of the spectroscopic transit of HAT-P-8 b motivated the scheduling of photometric observations of the transit, since the egress seemingly occurred several minutes before expectations on the 19 July 2010 sequence according to the ephemeris by Latham et al. (2009). Photometric observations to refine the ephemeris were therefore carried out from several sites in France and Spain on 25, 28, and 31 August, from both amateur and professional observatories, and are briefly described in Table 6. Each lightcurve was acquired and derived from observations independently; aperture photometry was performed with optimized parameters for each system and conditions. Additionally, a transit light curve obtained on the night of September 13th by Ken Hose, was recovered from the Extrasolar Transit Database (ETD).

The conversion from UTC timestamps to a barycentric dynamical time (TDB) standard was done using the code of Eastman et al. (2010). Although not mentioned explicitly in the discovery paper, the KeplerCam timestamps were assumed to be provided in UTC and were therefore corrected to TDB by adding 65.184 s to the measured central times (see Eastman et al. 2010). In all cases, this correction does not change the ephemeris above the 1-σ level.

Each light curve was fitted individually with the orbital and planetary parameters being fixed to those by Latham et al. (2009) in order to obtain the central times of transit. The error bars

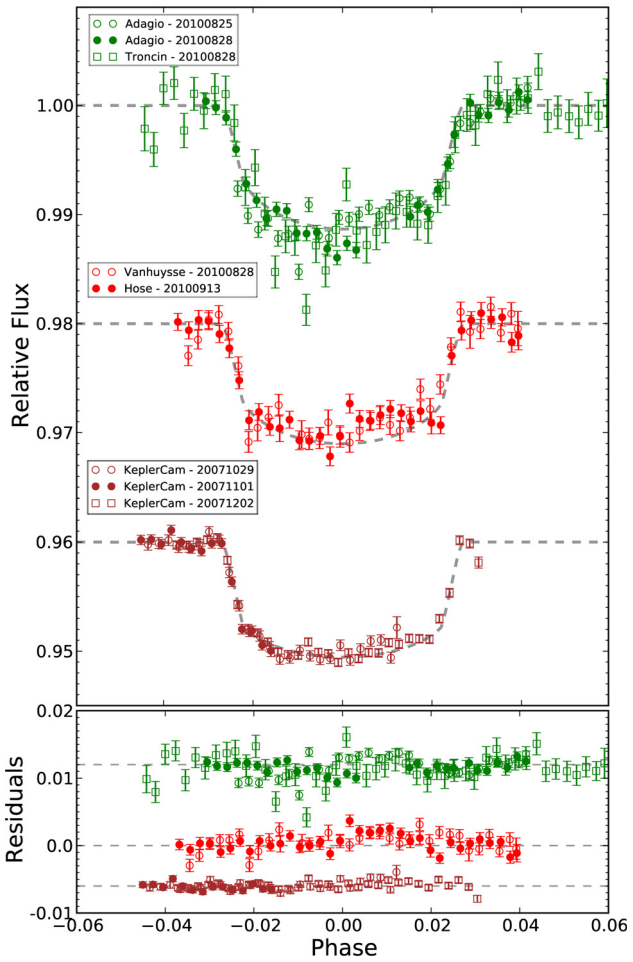

Fig. 2. *Upper panel*: transit light curves of HAT-P-8 in three different bands: V (*top*; green), R (*middle*; red), and Sloan-z (*bottom*; brown), shifted vertically to improve legibility. Different symbols indicate different observers or nights, as indicated in the legend. The dashed curve is the best-fit model for each photometric band. *Bottom panel*: residuals to the best-fit model. The data has been shifted to avoid crowding.

were estimated by means of the prayer bead method (see, for example, Désert et al. 2009), which consists of fitting a set of synthetic datasets obtained by shifting sequentially the residuals of the best-fit model rigidly and adding them back into the best-fit trapezoid function. The dispersion in the fit parameters obtained in this way is then used as an estimate of the uncertainties. This method permits us to preserve the structure of the residuals and is therefore supposed to produce error estimates that take into account the covariant noise in the light curves. At each iteration of the processes, the limb-darkening coefficient corresponding to each photometric band in which a transit was observed was drawn randomly from a normal distribution centred at the value obtained by interpolating the tables of Claret (2000) or Claret (2004) to the stellar parameters from Latham et al. (2009). The dispersion in this distribution is defined by the extreme values of the limb-darkening coefficients obtained by allowing the stellar parameters to vary within the reported 1-σ intervals. The KeplerCam lightcurves from the discovery paper (Latham et al. 2009) were fitted in a similar way. Figure 2 shows the light curves obtained by the different observers, together with the light curves from KeplerCam, binned to ten minutes.

An improved ephemeris was obtained by linear regression of the complete set of central times obtained, excluding the KeplerCam transit of 1 November 2007, since only the ingress was observed:

$$To[\mathrm{BJD} - 2\,450\,000] = 4437.67505 \pm 0.00042 \quad (1)$$

$$P = 3.0763373 \pm 0.0000031 \text{ days}, \quad (2)$$

with a covariance $\mathrm{cov}(P, To) = -5.1443 \times 10^{-10}$, and reduced $\chi^2 = 0.75$. The value of χ^2 probably means that the error bars of the central times of transits have been slightly overestimated. However, we decided not to scale them and hence report conservative ephemeris uncertainties.

This ephemeris is in good agreement with those obtained by Simpson et al. (2010), but the orbital period differs significantly (by almost 8-σ) from the value reported by Latham et al. (2009). As a consequence, the predictions for the 19 July transit differ by more than 19 min (8-σ). Using our computation, the expected central time of transit observed by SOPHIE is

$$T_c[BJD - 2\,450\,000] = 5397.49230 \pm 0.00089,$$

where the covariance was considered for propagating the error from the ephemeris.

To explore the disagreement with the prediction of Latham et al. (2009), we adjusted the data of this target obtained by the HATnet telescopes together with the KeplerCam transits, in an attempt to reproduce the ephemeris reported in the discovery paper. The orbital period thus obtained agrees with our measurement to the 2-σ level and differs from the period reported in Latham et al. (2009) by more than 7σ. We conclude (and we have verified afterwards with the author) there exists a problem – a misprint – with the value reported in Table 13 of Latham et al. (2009), and that the observed discrepancy is not real.

Using the above values for To and P, we adjusted the phase-folded curve using the analytical formulae of Mandel & Agol (2002) with a linear limb-darkening law to obtain the radius ratio $k = R_p/R_*$, the system scale a/R_*, and the impact parameter $b = a/R_* \cos(i)$. The minimum value of the χ^2 statistic was obtained using the down-hill simplex method (Nelder & Mead 1965), and the errors were estimated using the prayer bead method. At each iteration of the processes, the limb-darkening coefficient corresponding to each photometric band in which a transit was observed was drawn randomly from a normal distribution centred on the value obtained by interpolating the tables of Claret (2000) or Claret (2004) to the stellar parameters from Latham et al. (2009). The dispersion of this distribution is defined by the extreme values of the limb-darkening coefficients obtained by allowing the stellar parameters to vary within the reported 1-σ intervals.

The obtained parameters are in perfect agreement with those from Latham et al. (2009), although they have a larger uncertainty. We thus use the transit parameters of Latham et al. (2009) to model the spectroscopic transit.

4. Modeling the spectroscopic transits

We modelled the radial-velocity anomaly using the analytical approach developed by Ohta et al. (2005). The complete model has ten parameters: the four standard orbital parameters for circular orbits, the radius ratio R_p/R_*, the orbital semi-major axis to stellar radius a/R_* (constrained by the transit duration), the sky-projected angle between the stellar spin axis and the planetary orbital axis λ, the sky-projected stellar rotational velocity $v \sin i_s$, the orbital inclination i, and the linear limb-darkening coefficients based on Claret (2004) tables for filter g'. Our goal here is to measure the spin-orbit projected angle λ from the fits

of the RM anomaly shape; we thus allow the parameter λ to vary in the fits. As for HAT-P-6 (Hébrard et al. 2011), the parameters that have a significant impact on both the RM fits and the λ value are mainly the projected stellar velocity $v \sin i_s$ and the systemic velocity γ of the data, in addition to and less critically, the RV semi-amplitude K and orbital inclination i. The K and i parameters were fixed to their mean value in the fit but we explored the range in their error bars and quadratically added their small contribution to the final errors in $v \sin i_s$ and λ. We constructed a grid scanning the different values for λ, $v \sin i_s$, and the systemic velocity γ, and computed the χ^2 for each model. We performed a conservative re-scaling of the χ^2 array, introducing a correction for the χ^2 fluctuations due to the limited number of degrees of freedom, as explained in Hébrard et al. (2002). Adopting the minimum χ^2 obtained for each value on the grid of a given parameter (e.g. λ), we determined the uncertainty in this parameter from the χ^2 and $\Delta\chi^2$ variations of 1, 4, and 9 determining the interval confidences at 1, 2, and 3σ.

In the RM fits, the degeneracy between $v \sin i_s$ and λ increases with the orbital inclination i. For impact parameters b that are not too small, this correlation was taken into account in this work, by exploring the entire space of possible values for $v \sin i_s$ and λ. Figure 3 shows a zoomed view of the spectroscopic transits and their best-fit solutions. The confidence interval contours estimated from the rescaled-χ^2 variations against λ and $v \sin i_s$ are plotted in Fig. 4.

4.1. HAT-P-8

We used the orbital parameters derived in Sects. 2.1 and 3 and the transit parameters from Latham et al. (2009). Two datasets were used to search for the best-fit solution: first, the SOPHIE data set (35 measurements during the transit night), as described in Sect. 2.1; second, the data set composed of the SOPHIE data, in addition to the FIES measurements published by Simpson et al. (2010), which include a total of 28 data points. When quadratically adding 15 m/s to the FIES individual errors (as in Simpson et al. 2010), and allowing for a free offset between both SOPHIE and FIES data sets, we obtained values of $v \sin i_s = 14.5 \pm 0.8$ km s^{-1}, $\lambda = -17° \pm 8°$ for the projected rotational velocity and spin-orbit angle, respectively, with a reduced χ^2 of 1.19. Fits with the extreme values of i show that an additional uncertainty should be quadratically added to the uncertainty obtained from the χ^2 variations. We verified that, as expected, variations in other parameters within their error bars have no significant impact on λ. The final value of λ is $-17^{\circ}{}^{+9.2}_{-11.5}$.

The values reported by Simpson et al. (2010) are –9.7° for λ (1-σ range from –17.4° to –0.7°) and 11.8 ± 0.5 km s^{-1} for $v \sin i_s$. Adding the SOPHIE values therefore tended to slightly increase the spin-orbit angle (both estimates being in agreement within 1-σ), while the derived $v \sin i_s$ increased by about 2-σ. It is a known consequence of fitting the spectroscopic transits of stars that are significantly rotationally broadened, that the $v \sin i_s$ is over-estimated (Hirano et al. 2010), with consequences for the estimated λ value that are of order of magnitude smaller than our error bar (Triaud et al. 2009). Figure 4 shows the distribution of χ^2 values against λ for this system.

4.2. HAT-P-9

We first attempted to fit the planetary orbit, using the full set of SOPHIE data since 2007, and new ephemeris data by Dittmann et al. (2010): we found a smaller dispersion in the residuals and a planetary mass that is slightly lower than that given in Shporer et al. (2009). The RV best-fit semi-amplitude is $K = 73.8 \pm 6.7$ m/s and $M_p = 0.67 \pm 0.08\ M_{Jup}$ with $M_s = 1.28 \pm 0.13\ M_\odot$.

For this planet, the semi-amplitude of the RM anomaly is larger than the amplitude of the orbital motion, a rare situation again explained by the large planetary radius, large stellar rotational velocity, and relatively low mass of the planet (hence small orbital amplitude). The Rossiter effect is then modelled

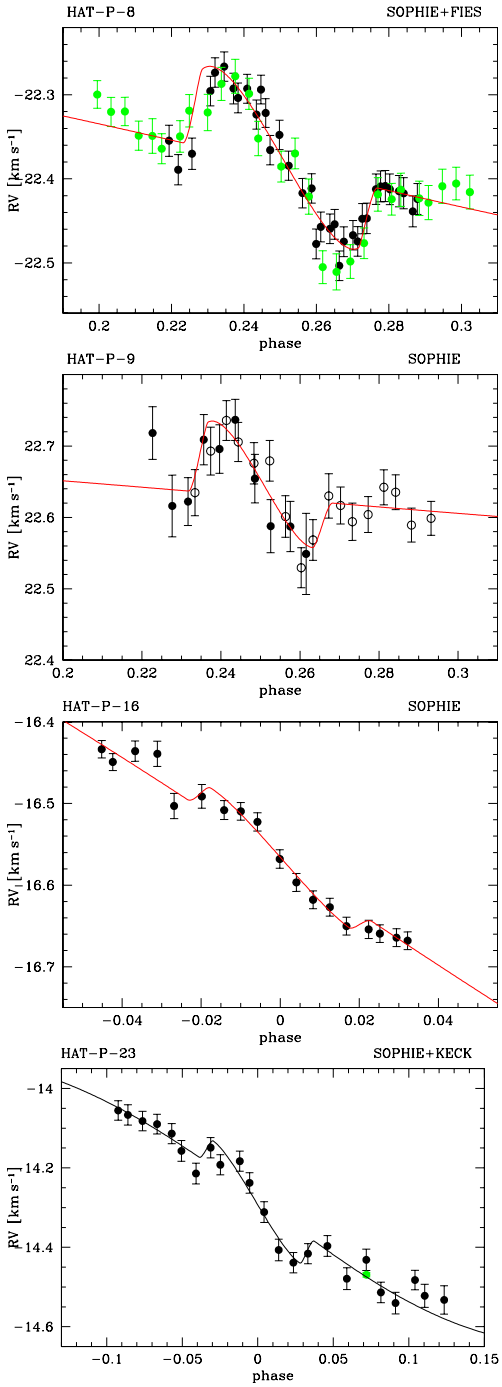

Fig. 3. Close-up view of the radial-velocity measurements of HAT-P-8, HAT-P-9, HAT-P-16, and HAT-P-23 obtained with SOPHIE during transit nights. The best-fit Rossiter-McLaughlin models are superimposed as a red dashed line. FIES data of HAT-P-8 are included as green circles (Simpson et al. 2010). Data for two separate observing nights are shown with different symbols for HAT-P-9 (filled circles: 28 December 2010, open circles: 1 January 2011).

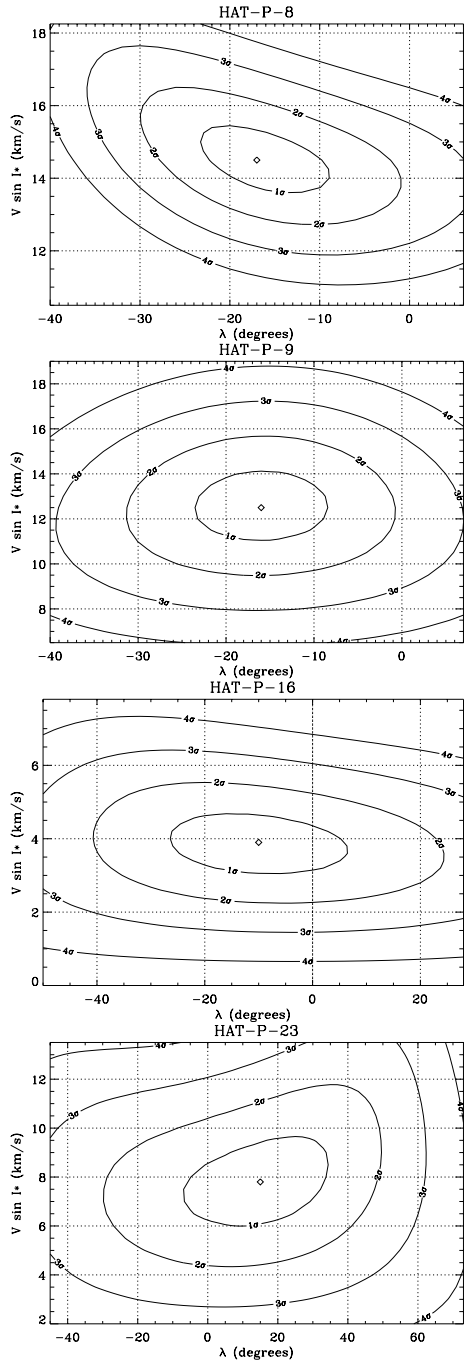

Fig. 4. χ^2 contour plot for the λ values from the Rossiter-McLaughlin fits.

by combining both the December 2010 and January 2011 data sequences, and allowing a free offset between these series. Half of the transit was observed twice, so that the offset is determined from a subset of about eight measurements per series. An offset of 37 m/s was found to minimize the residuals. With the total sample of 27 measurements during or close to the transit, the best-fit solution of the Rossiter-McLaughlin anomaly corresponds to a rotational velocity of 12.5 ± 1.8 km s^{-1} (in agreement with Shporer et al. 2009) and spin-orbit angle λ of $-16° \pm 8°$. The reduced χ^2 value is 0.68. Taking into account the impact of the RV semi-amplitude and inclination errors significantly changes neither the value nor its error bar. The transit data and its best-fit solution are shown in Fig. 3, and the χ^2 distribution of the derived quantity is shown in Fig. 4.

4.3. HAT-P-16

Owing to a lower value of the stellar rotational velocity and a non-inflated planet, the amplitude of the Rossiter anomaly on the star HAT-P-16 is small, while the individual measurement precision is greater than for the other sequences. We performed the fit using the transit parameters derived by Buchhave et al. (2010) and found a best-fit solution for a stellar projected rotational velocity of 3.9 ± 0.8 km s^{-1} (in agreement with Buchhave et al. 2010) and a spin-orbit angle of -10 ± 16 °. The reduced χ^2 of the fit is 0.89, and the fitted data and χ^2 distribution are shown in Figs. 3 and 4. We checked that the variation in the RV semi-amplitude and inclination within their error bars did not have a noticeable impact on the value and error in the spin-orbit angle and rotational velocity in this case. We note that with an effective temperature of 6158 K, one may expect the stellar rotational velocity to be greater than 3.9 km s^{-1}. An average value for such a star should instead be about 10 km s^{-1} (Nordström et al. 2004). It is thus possible that the stellar rotation axis of HAT-P-16 is inclined to the line of sight, resulting in a real spin-orbit angle that is larger than measured.

4.4. HAT-P-23

Finally, the SOPHIE data of HAT-P-23 were adjusted in the same way as previously, using the transit parameters and ephemeris of Bakos et al. (2010). We derived a stellar rotational velocity of 7.8 ± 1.6 km s^{-1} and a projected angle between the orbital plane and the stellar equatorial plane, of $15° \pm 22°$. We again verified how the variations in the RV semi-amplitude and inclination within their error bars would affect the value and error in the spin-orbit angle and rotational velocity; in this case, the error in the inclination had some impact, which was included in the final error bars. The $v \sin i_s$ derived from the fit is in good agreement with the value reported in Bakos et al. (2010) from stellar analyses. Figure 4 shows the χ^2 distribution as a function of λ.

5. Discussion

Table 7 summarizes the values derived from our analyses of the spectroscopic transits of HAT-P-8 b, HAT-P-9 b, HAT-P-16 b, and HAT-P-23 b. The total number of systems with published projected spin-orbit angles is now 37. Ten of them are in the range $|\lambda| = 20$–$120°$, 7 are retrograde (more than ~120°), 22 are less than ~20°, among them being the four systems presented here. We recall that the λ value is the projected spin-orbit angle. The analysis of the real spin-orbit angle ψ distribution by Triaud et al. (2010) showed that between 45% and 85% of hot Jupiters may have an orbital inclination greater than 30°. Schlaufman (2010) discussed the projected stellar rotation axis and the spin-orbit measurements and concluded that systems of massive stars and planets are more likely to show an apparent misalignment.

Since the discovery of the first misaligned system (Hébrard et al. 2008), many processes have been invoked to explain them: the three-body Kozai mechanism (Fabrycky & Tremaine 2007), planet-planet scattering (Chatterjee et al. 2008; Ford & Rasio 2008), tilted disks (Bate et al. 2010; Lai et al. 2011), and insufficient tidal torque of stars hotter than 6200 K – hence a conservation of an original misalignment caused by mechanisms acting on planets around hot stars (Winn et al. 2010a). Another

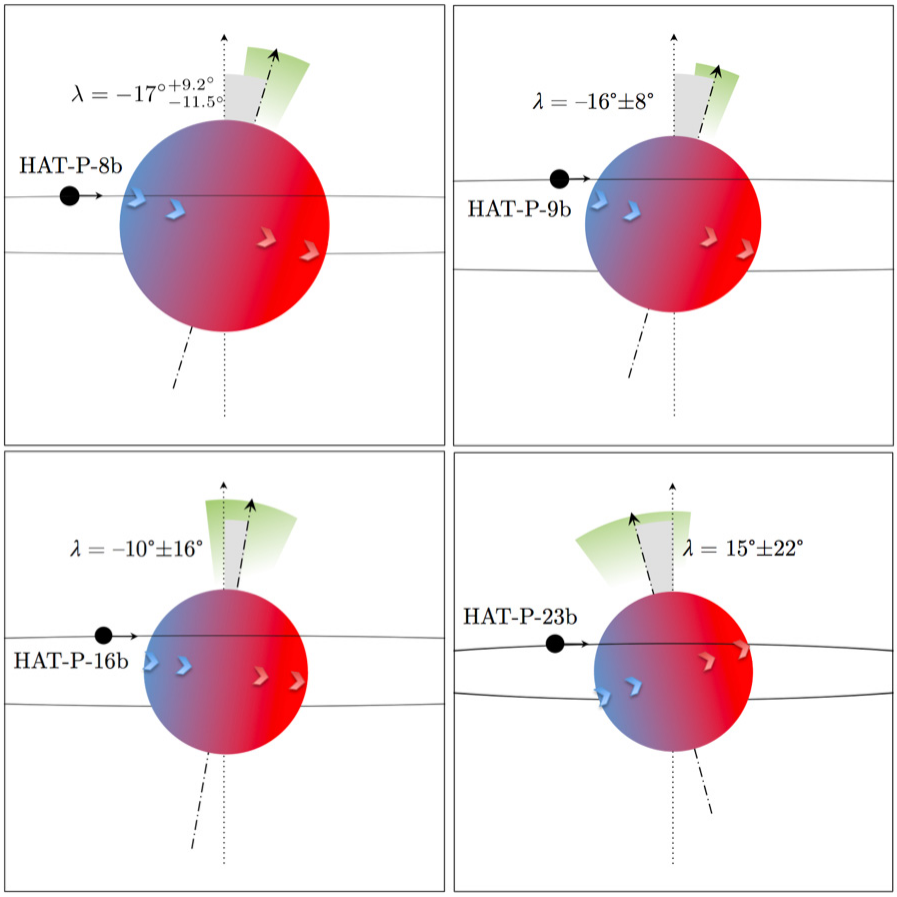

Fig. 5. Sketch of the orbital and rotational orientations for all four systems discussed here, as viewed from Earth.

Table 6. Photometric observations of the transits of HAT-P-8 b used to refine the ephemeris.

Observer	Location	Instrument	Photometric band	Date of transit obs.
Assoc. Adagio	Toulouse, F	82-cm, SBIG STL-6303E	*V*	08.28.10 and 08.31.10
Hose	Portland, Oregon	32-cm, QSI 516wsg	*R*	09.13.10
Troncin	OHP, F	120-cm Tektronix TK1024	*V*	08.28.10
Vanhuysse	La Palma, S	35-cm, SBIG STL-1001e	*R*	08.28.10

Table 7. Spectroscopic transit modelled parameters of HAT-P-8, HAT-P-9, HAT-P-16, and HAT-P-23.

Star	V_0 km s^{-1}	$v \sin i_s$ km s^{-1}	λ degrees	χ^2_{red}	T_{eff} K	M_p M_{Jup}
HAT-P-8	–22.384 ± 0.0035	14.5 ±0.8	–17 (–11.5, +9.2)	1.19	6200 ± 80	1.52±0.18
HAT-P-9	+22.628 ± 0.008	12.5 ±1.8	–16 ± 8	0.68	6350 ± 150	0.67 ± 0.08
HAT-P-16	–16.553 ± 0.0035	3.9 ± 0.8	–10.0 ± 16	0.89	6158 ± 80	4.193 ± 0.094
HAT-P-23	–14.259 ± 0.007	7.8 ± 1.6	+15 ± 22	1.02	5905 ± 80	2.09 ± 0.11

Notes. Effective temperatures and planetary masses are taken from the discovery papers, except the planet mass of HAT-P-9 which is re-estimated in this work.

process that should be taken into account in this global picture is the tidal instability, which may affect all systems by tilting the rotation axis of the star on relatively short timescales (Cébron et al. 2011), thus contribute to the distribution of orbital inclinations. The four systems analysed in this paper seem to be outside the so-called forbidden zone – which is defined by an orbital period shorter than one third of the stellar rotational period (Le Bars et al. 2010), and where the tidal instability cannot grow, thus might have suffered a change in obliquity during their history. Complete simulations of the tidal evolution of the systems should be carried out in order to unveil the possible impact of the tides on the stars or the planets, particularly HAT-P-16 and HAT-P-23 , which exhibit a non-zero eccentricity despite their age (2.0 and 4.0 Gyr, respectively).

It is thus almost easier now to explain misaligned systems, than the more abundant hot Jupiters close to alignment. The addition of four systems that are not strongly misaligned, as well as other discoveries renews our interest in this majority of systems that are "surviving" the vast range of possible causes of misalignment. Why should hot Jupiters be aligned with the equator

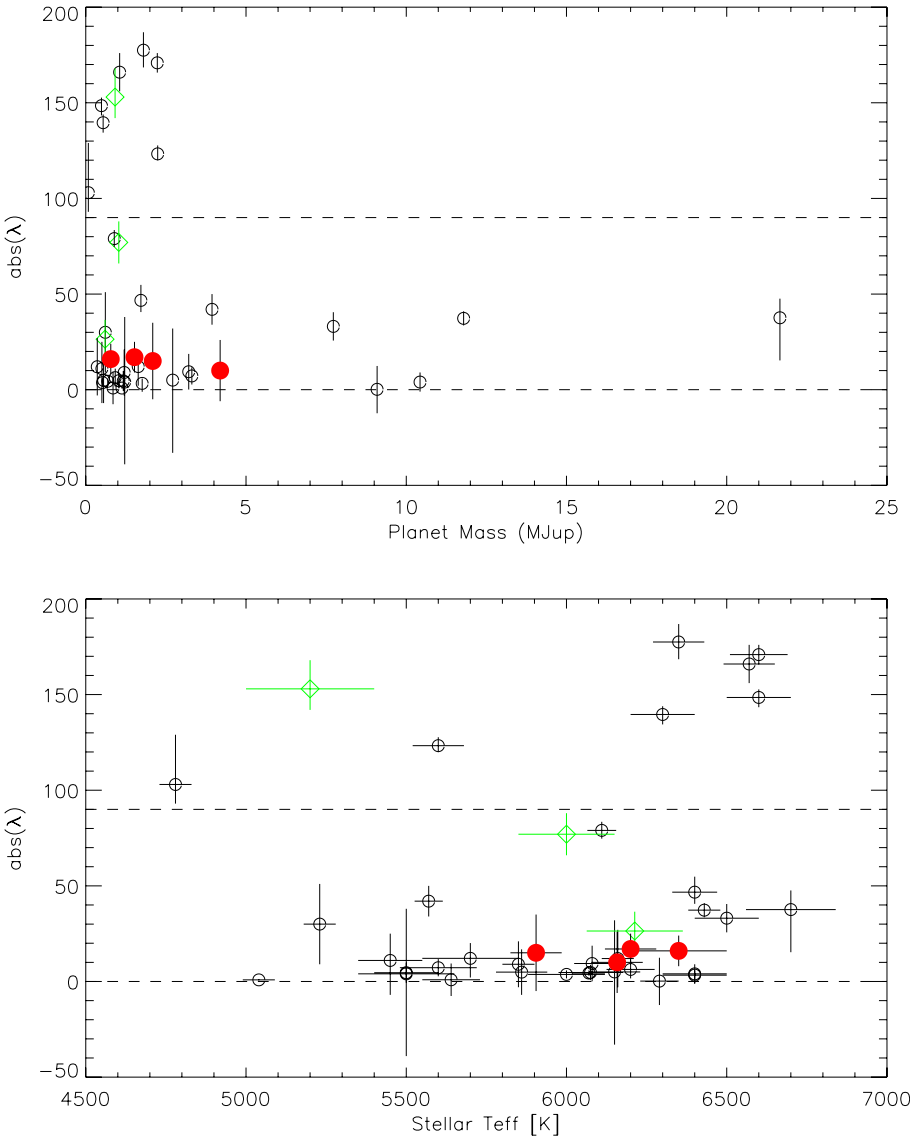

Fig. 6. Absolute value of the spin-orbit angle as a function of planetary mass (*top*) up to 25 $M_{\rm Jup}$ and stellar effective temperature (*bottom*). The red filled large symbols show the new measurements. The uncertain values for CoRoT-1b, WASP-2, and Kepler-8 are included as green unfilled rhombus symbols.

of their star, and which parameter(s) would permit us to predict the behaviour of the orbital planes? What constraint do we have on the sample of the aligned hot Jupiters, in terms of the exclusion of other planets or stellar companions in the system, or stellar and disk properties?

Figure 6 (top) shows the distribution of the absolute value of the λ projected spin-orbit angle with respect to the planetary mass, updated from a similar plot by Hébrard et al. (2010) with almost a factor of two more systems. It shows that most of the systems have a low projected spin-orbit angle over the mass range of Jupiter-like planets. Among the planets in this mass range with misaligned orbits are planets in binary systems (such as WASP-8, Queloz et al. 2010) and seven systems in retrograde orbits ($|\lambda| > 100°$). These latter systems show some dependence on the planetary mass, only planets less massive than 3 $M_{\rm Jup}$ being retrograde.

Our conclusions at the moment are that there are i) notable exceptions to any general rule (e.g. HAT-P-11 announced by Winn et al. (2010b), that has a $\lambda = 103°$ orbit around a cool star, which appears to be linked to the tidal dissipation rather than the effective temperature of the star); and ii) partial pieces of knowledge of the systems (unknown additional planets or stellar companions in the systems), that limit our understanding of the common behaviour. Figure 6 (bottom) shows an updated version of the $|\lambda|$ dependence with stellar effective temperature, as in Winn et al. (2010a). Our data might add a new exception to the rule that hot stars have planets with high obliquities (HAT-P-9 is has a low-angle misalignment, compatible at 2-σ with zero with $T_{\rm eff} = 6350$ K), although it may also indicate that the obliquity has never changed during the system's evolution. In addition, two of the systems reported in this paper lie close to the limiting temperature proposed by Winn et al. (2010b), HAT-P-8 and HAT-P-16 (with $T_{\rm eff} = 6200$ and 6158 K, respectively). Finally, HAT-P-23 with a cooler star ($T_{\rm eff} = 5905$ K) and aligned orbit is representative of the majority of these systems. The current sample of planets with measured spin-orbit projection angles hinders statistically significant conclusions about the difference between planets orbiting hot and cold host stars from being drawn. When considering $T_{\rm eff} = 6250$ K as the limiting temperature between samples, a Kolmogorov-Smirnov test on the data fails at rejecting the null hypothesis (i.e. that the sample of measured λ for hot and cold systems are drawn from the same distribution) with a significance below $\alpha = 0.11^{+0.17}_{-0.09}$, where the error bars are inferred from 10 000 bootstrap realisations of the data, using the uncertainties in the effective temperature and λ reported in the literature. This means that at the 1-σ level, there exists a 28%

chance of erroneously rejecting the hypothesis that both populations are one and the same. Interestingly, we found slightly lower values for the significance when the limiting $T_{\rm eff}$ is slightly higher: for $T_{\rm eff}$ between 6300 K and 6450 K, the null hypothesis can be rejected at the 1-σ level with a significance $\alpha = 0.2$. We note, however, that for these temperatures only about ten systems are classified as orbiting hot stars.

The first steps are thus to systematically complete our understanding of the systems, by both following up known transiting hot Jupiters by monitoring their radial velocity over an extended period, and by deriving the detection limits of stellar companions by direct imaging. Companions capable of significantly misaligning the planetary systems through Kozai oscillations should generally be separated by no more than ∼100 AU from the stars hosting the planets, otherwise the Kozai period exceeds that of the relativistic precession leading to a dampening of the Kozai cycles (Fabrycky & Tremaine 2007). Unfortunately, the transiting systems discovered during surveys such as HATnet or SuperWASP are commonly located at large distances (>200 pc). Consequently, adaptive optics imaging surveys such as the ones carried out at Subaru (Narita et al. 2010) or VLT (Ehrenreich et al., in prep.) have to probe the stellar environment to within a few 0.1 arcsec. Searching for low-mass stars or brown dwarfs at these separations requires the use of innovative techniques such as angular differential imaging or sparse aperture masking (Lacour et al., in prep.). Alternatively, these companions could be detected by measuring a long-term drift in the radial velocity of the star, provided that they are observed long enough. A systematic collection of such data would provide useful constraints on the multi-body mechanisms and thus help us to differentiate between all other proposed scenarios for single planets around single stars.

Acknowledgements. We wish to thank to the referee Josh Winn for his very helpful remarks that greatly improved the paper. We gratefully acknowledge the Programme National de Planétologie (telescope time attribution and financial support), the Swiss National Foundation, and the Agence Nationale de la Recherche (grant ANR-08-JCJC-0102-01) for their support. D.E. is supported by CNES. We warmly thank the OHP staff for their great care in optimising the observations. N.C.S. acknowledges the support of the European Research Council/European Community under the FP7 through Starting Grant agreement number 239953. N.C.S. also acknowledges the support from Fundação para a Ciência e a Tecnologia (FCT) through program Ciência 2007 funded by FCT/MCTES (Portugal) and POPH/FSE (EC), and in the form of grants reference PTDC/CTE-AST/66643/2006 and PTDC/CTE-AST/098528/2008. A.E. is supported by a fellowship for advanced researchers from the Swiss National Science Foundation.

References

Bakos, G. Á., Lázár, J., Papp, I., Sári, P., & Green, E. M. 2002, PASP, 114, 974
Bakos, G., Noyes, R. W., Kovács, G., et al. 2004, PASP, 116, 266
Bakos, G. Á., Hartman, J., Torres, G., et al. 2010, ApJ, submitted [arXiv:1008.3388]
Bakos, G. Á., Hartman, J. D., Torres, G., et al. 2011, in Detection and Dynamics of Transiting Exoplanets, St. Michel l'Observatoire, France, ed. F. Bouchy, R. Díaz, & C. Moutou, EpJ Web Conf., 11, id. 01002
Baranne, A., Queloz, D., Mayor, M., et al. 1996, A&AS, 119, 373
Bate, M. R., Lodato, G., & Pringle, J. E. 2010, MNRAS, 401, 1505
Boisse, I., Eggenberger, A., Santos, N. C., et al. 2010, A&A, 523, A88
Bouchy, F., Hébrard, G., Udry, S., et al. A. 2009a, A&A, 505, 853
Bouchy, F., Isambert, J., Lovis, C., et al. 2009b, in EAS Publ. Ser., 37, ed. P. Kern, 247
Buchhave, L. A., Bakos, G. Á., Hartman, J. D., et al. 2010, ApJ, 720, 1118
Cébron, D., Moutou, C., Le Bars, M., Le Gal, P., & Fares, R. 2011, in Detection and Dynamics of Transiting Exoplanets, St. Michel l'Observatoire, France, ed. F. Bouchy, R. Díaz, & C. Moutou, EPJ Web Conf., 11, id. 03003
Chatterjee, S., Ford, E. B., Matsumura, S., & Rasio, F. A. 2008, ApJ, 686, 580
Claret, A. 2000, A&A, 363, 1081
Claret, A. 2004, A&A, 428, 1001
Désert, J., Lecavelier des Etangs, A., Hébrard, G., et al. 2009, ApJ, 699, 478
Dittmann, J. A., Close, L. M., Scuderi, L. J., Turner, J., & Stephenson, P. C. 2010 [arXiv:1006.3580]
Eastman, J., Siverd, R., & Gaudi, B. S. 2010, PASP, 122, 935
Fabrycky, D., & Tremaine, S. 2007, ApJ, 669, 1298
Ford, E. B., & Rasio, F. A. 2008, ApJ, 686, 621
Hébrard, G., Lemoine, M., Vidal-Madjar, A., et al. 2002, ApJS, 140, 103
Hébrard, G., Bouchy, F., Pont, F., et al. 2008, A&A, 488, 763
Hébrard, G., Désert, J., Díaz, R. F., et al. 2010, A&A, 516, A95
Hébrard, G., Ehrenreich, D., Bouchy, F., et al. 2011, A&A, 527, L11
Hirano, T., Suto, Y., Taruya, A., et al. 2010, ApJ, 709, 458
Lai, D., Foucart, F., & Lin, D. N. C. 2011, MNRAS, 412, 2790
Latham, D. W., Bakos, G. Á., Torres, G., et al. 2009, ApJ, 704, 1107
Le Bars, M., Lacaze, L., Le Dizès, S., Le Gal, P., & Rieutord, M. 2010, Phys. Earth Plan. Inter., 178, 48
Mandel, K., & Agol, E. 2002, ApJ, 580, L171
Narita, N., Kudo, T., Bergfors, C., et al. 2010, PASJ, 62, 779
Nelder, J., & Mead, R. 1965, Comp. J., 7, 308
Nordström, B., Mayor, M., Andersen, J., et al. 2004, A&A, 418, 989
Ohta, Y., Taruya, A., & Suto, Y. 2005, ApJ, 622, 1118
Perruchot, S., Kohler, D., Bouchy, F., et al. 2008, SPIE Conf., 7014
Queloz, D., Anderson, D., Collier Cameron, A., et al. 2010, A&A, 517, L1
Rossiter, R. A. 1924, ApJ, 60, 15
Schlaufman, K. C. 2010, ApJ, 719, 602
Shporer, A., Bakos, G. Á., Bouchy, F., et al. 2009, ApJ, 690, 1393
Simpson, E. K., Pollacco, D., Collier Cameron, A., et al. 2011, MNRAS, 414, 3023
Triaud, A. H. M. J., Queloz, D., Bouchy, F., et al. 2009, A&A, 506, 377
Triaud, A. H. M. J., Collier Cameron, A., Queloz, D., et al. 2010, A&A, 524, A25
Winn, J. N., Fabrycky, D., Albrecht, S., & Johnson, J. A. 2010a, ApJ, 718, L145
Winn, J. N., Johnson, J. A., Howard, A. W., et al. 2010b, ApJ, 723, L223